ISSN: 2834-7749

Research Article

Insights of Herbal Medicine

# Excitation-Induced Conformational Changes in ecDHFR: Attenuable Luminance Element in Instant Reaction States

**Chia Yu, Chang[1]*, Ronnie E, Thebeau[2] and Fang Yu, Chang[3]**

[1]*Institute of Biotechnology, Department of Biological Science and Technology, National Yang Ming Chiao Tung University*

[2]*Institute of System Design and Management Department, Massachusetts Institute of Technology*

[3]*Institute of Electrophysics, National Yang Ming Chiao Tung University*

***Corresponding Author**
Chia Yu, Chang, Institute of Biotechnology, Department of Biological Science and Technology, National Yang Ming Chiao Tung University.

**Submitted:** 2024, Apl 12; **Accepted:** 2024, May 01; **Published:** 2024, Aug 13

**Citation:** Chang, C. Y., Thebeau, R. E., Chang, F. Y. (2024). Excitation-Induced Conformational Changes in ecDHFR: Attenuable Luminance Element in Instant Reaction States. *Insights Herbal Med, 3*(3), 01-19

## Abstract

*Escherichia coli dihydrofolate reductase (ecDHFR) is an enzyme that synthesizes 5,6,7,8- tetrahydrofolate a kind of crucial compound involved in nucleotide biosynthesis. Recent research has shown that when ecDHFR undergoes specific reactions and subsequently exposed to excitation, it is transformed into a stable fluorescent protein. Complexes formed involving dihydrofolate, NADPH inside wild-type and mutants ecDHFR with an ionic $NADPH^+$ and tetrahydrofolate under Arrhenius acid solutions have exhibited electronic resonance effects. These findings suggest that microscale reactions are governed by specific potential energies form bind formation, electrostatic attraction, ionic force in the hydrophobic steady state. In Computed Tomography, tracers' move forward, the ability to generate realistic excitation response ratios and compare the wild-type and mutant ecDHFR before and after reactions will provide further insights into the dynamic protein structure workings of ecDHFR and its relationship with image formation capability under micro solution.*

***Graphic Abstract***

*The ecDHFR reaction complex forms binding procedure and reaction mechanism.*

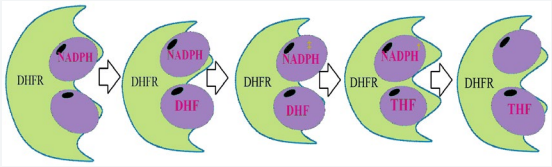


**Keywords:** Steady State Potential, Dihydrofolate Reductase, Fluorescence, Bio-Probe

## 1. Introduction

The dihydrofolate reductase (DHFR) gene, belonging to the oxidoreductase family, is located on chromosome 5 at the nonfunctional locus [1]. The role of DHFR to catalyze reactions on the pteridine group (*p*-ABA, amino benzoate), which serve as the precursor for nucleotide synthesis, existing in both conjugated and nonconjugate forms [2]. DHFR uses 7,8-dihydrofolate folate (DHF, ($H_2$-folate)) to synthesize 5,6,7,8-tetrahyfolate (THF, ($H_4$-folate)). Moreover, the stereochemistry at $C^6$ of the biologically active diastereoisomer of folic acid has been defined via NMR. The conversion of DHF to THF produces a diastereomer at the $C_6$ center, from $[\alpha]_D^{32}$ = -49.9$^0$ in 1.5 M Tris containing 0.2 M ethanethiol to $[\alpha]_D^{32}$= -16.9$^0$ (S). However, the stereocenter of $C_7$ remains unidentified the biological characters, but reduction

also caused *re*-face to *si*-face at $C_7$ of folic acid [3]. There are many studies on the DHFR reaction. DHFR can form three distinct molecular complexes: DHFR-DHF complex, DHFR, nicotinamide adenine dinucleotide phosphate ($NADP^+$) complex, and DHFR,DHF,$NADP^+$ catalytic complex (Supplementary 3 (1), (2), and (3)). Type II DHFR forms a DHFR•DHF•$NADP^+$ catalytic complex, which has been resolved at 1.26 Å [4]. This structure comprises three pairs of *cis*-parallel and one pair of *trans*-parallel β sheets. Surrounding these sheets are four α-helices, giving DHFR a unique spherical conformer. Additionally, the structure features flexible loops, including the M20 loop (residues 20 and 23) and the FG loop in the I-α-β motifs (residues 120-125).

These dissociation and structure studies play a crucial role in the enzymatic activity and catalytic function of DHFR [5]. In the catalyst complex, the polar backbone atoms of two symmetry-related I68 residues provide recognition motifs and interacting with carboxamide on the nicotinamide ring and the $N^3$-$O^4$ amide function on the pteridine ring, respectively. This set of interactions orients the atomic rings of substrate and cofactor in a relative endo geometry [4]. Another study shows the formation of a DHFR, methotrexate•-, $NADP^+$ catalytic complex, resolved at a resolution of 2.1 Å. In this complex, an M20 loop (residues 20 and 23) is predominantly closed over the reactants in the holoenzyme, Michaelis, and transition state complexes. However, when the M20 loop transitions from a close to an occluded state, the central portion of the loop rearranges from β-sheet to $3^{10}$ helices [6]. From this finding to say, four mutant clones were designed to induce micro-conformation attenuation in DHFR. Each mutant clone, T113C with W30C and M42C with W47C, introduced artificial linkages between different residues, resulting in altered protein flexibility. The micro-conformation differences have varying effects on entropy, electrostatic force in each mutant. The formation of the DHFR complex is influenced by these energies change and the electrostatic forces. Especially the fluorescence of DHFR can be altered quenched by different molecule entries.

The fluorescence intensity is also affected by the presence of NADPH, which can form resonance with the DHFR owing to the electrophilic nature of NADPH. However, when DHF enters the system, the fluorescence intensity shows a concentration-dependent relationship with DHF molecule concentration. DHF, despite having high background emission properties, can induce internal energy shifts or resonance with DHFR. The substrate binding was performed to build up the affinity ability on substrate and enzyme complex.

## 2. Experiment Methods

### 2.1 Plasmid Design, Protein Expression, and Protein Purification

The *Escherichia Coli* DHRF sequence (ecDHFR Uniprot: P0ABQ4) with the the N- treminal insertion to the following list: The plasmid was subcloned into subcloned into the BamHI and EcoRI sites of the pRSETa plasmid. The resulting pRESTabioseq-ecDHFR plasmid was created using DNA synthesis services by Genscript with DNA sequence confirmation. Owing to low expression levels, the bioseq- ecDHFR DNA sequence was further subcloned into the BamHI and EcoRI sites of the pET28a plasmid, forming the pET28a bioseqec-ecDHFR construct. This new construct was used to express ecDHFR with some modifications compared to a previous report. Briefly, E. coli BL21(DE3)-pLysS cells containing the pET28a-bioseq-ecDHFR construct were cultured at 37°C in LB broth containing 50 mg/L kanamycin until reaching an absorption of 0.6 at 600 nm. Subsequently, the cells were induced at 37°C for 5−8 h with 0.3 mM isopropyl-*β*-*D*-1-thiogalactopyranoside (IPTG). After harvesting, the 6 Histag bioseq- ecDHFR protein was purified using an ÄKTA prime plus liquid chromatography system with His-Trap high-performance columns (Ni Sepharose affinity resin) followed by a Hiprep-26/60 desalting column. Elution was achieved via a gradient of 10- 500 mM imidazole in 50 mM phosphate-buffered saline containing 500 mM NaCl at pH 8.0, resulting in the elution of the bioseq-ecDHFR protein was eluted between 150 and 255- mM imidazole. After desalting and dialysis, the 6Histag-bioseq-ecDHFR protein was stored in MTEN buffer which was compromising of 50 mM 2-(N-morphoholino (MES), 25 mM Tris, 100 mM NaCl, 0.1 mM EDTA, and 25 mM ethanolamine at pH 7.4. All enzyme and ligand-binding assays were performed within 3 days of storage at 4°C. Specific amino acids positions from catalytic nearby to the farest site, three highly conserved positions, Methionine 42 (M42), Tryptophan 47 (W47C), and Threonine 113 (T113), were selected. Then, the QuikChange Lightning Site-directed Mutagenesis kit (StrateGene) was used to introduced single-point mutations, resulting in the following mutants: W30C-ecDHFR, M42C-ecDHFR, and T113C-ecDHFR.

### 2.2 Investigation of the Enzyme Activity

To quantify ecDHFR, UV280 spectrum analysis was performed. Subsequently, a mixture of 5 μM DHFR, 10 μM NADPH, and 50 μM DHF was combined, and its absorbance was recorded at 340 nm, 282nm, 280 nm comparing them with the blank sample containing only ecDHFR and DHF while maintaining the temperature at $25^0$C. Hitachi double-beam spectrophotometer (U-3900) was used for the measurement.

### 2.3 Substrate and Enzyme Binding Assay

The ecDHFR protein contains five intrinsic tryptophan residues (W47C/M42C/T113C). A suitable line for NADPH was established via series titration. Then, the wild-type and the mutant, at a concentration of ecDHFR 5 μM, were added to dihydrofolate, NADPH in the substrate- ecDHFR, cofactor ecDHFR binding complex formation experiment. Each compound had its respective absorbance coefficient is as follows: NADPH (ε340 = 6.22 $mM^{-1}$ $cm^{-1}$), DHF (ε282 = 28 $mM^{-1}$ $cm^{-1}$). Under 340 nm excitation, by 290 nm irradiation, ecDHFR exhibits fluorescence within 420–460 nm, with an emission peak at 360 nm. The equilibrium affinity constant ($K_D$) was determined via titration with increasing DHF and NADPH concentration. Each substrate and cofactor binding with the enzyme was performed in triplicate.

### 2.4 UV and Fluorescence Spectroscopic Analyses: Determination of Concentration, Excitation Level, and Complex Formation

Using 290 nm as the excitation wavelength, ecDHFR exhibited emission peaks within 300-460 nm which arises from five tryptophan residues in the ecDHFR, protein, with each being close (<16 Å) to its neighboring tryptophan residues. This short distance between the tryptophan residues facilitates the enzyme complex formation. However, compounds, such as DHF, and THF do not considerably impact this phenomenon owing to the quenching effect observed as the substrate concentration increases. The UV spectrum shows two characteristic peaks, one at 300 -570 nm and the other located at 340 nm. The former exhibits a slight blue-shift, and the later shows a red- shift. These spectral shifts allow us to construct a binding saturation curve using the Origin program. Both $\Delta F_{340}$ and $\Delta F_{440}$ can be used as data sources for this analysis, but for supplementary information, $\Delta F_{340}$ was used.

## 3. Results and Discussion

### 3.1 Substrate and Enzyme Binding

The $K_D$ ratio of wild type was 2.61 ± 0.42 µM, as shown in Fig. 1F, 1G.

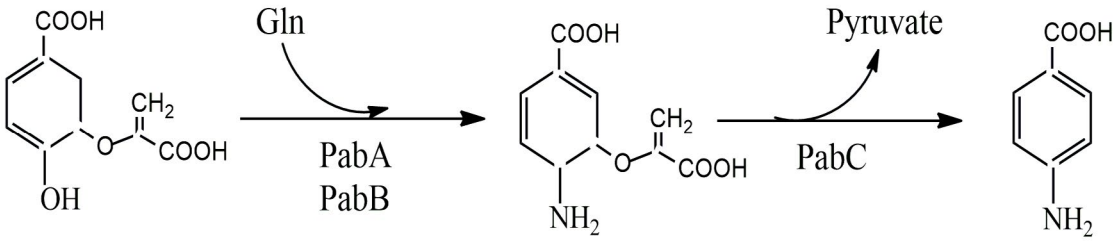


**Figure 1A**

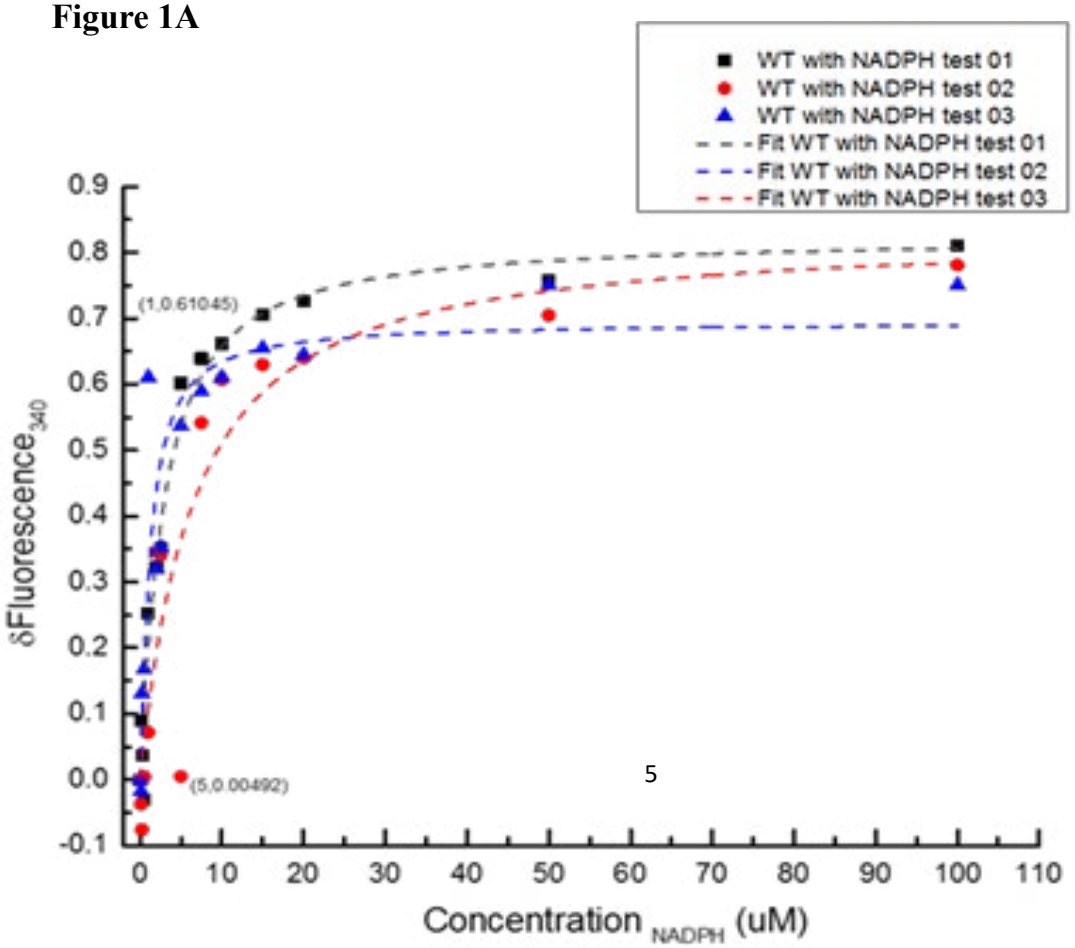


**Figure 1F (1):** The fluorescence emissions for the formation complex of WT ecDHFR with different NADPH concentrations (0, 0.1, 0.25, 0.5, 1, 2, 2.5, 5.0, 7.5, 10, 15, 20, 50, and 100 µM) under emission 290 nm.

**Figure 1F (2)**
The fluorescence emissions for the formation complex of T113C ecDHFR with different NADPH concentrations (0, 0.1, 0.25, 0.5, 1, 2, 2.5, 5.0, 7.5, 10, 15, 20, 50, 120, 180, 200, 220, 250, and 270 μM) under emission 290 nm for triplicate experiments at different times. Fluorescence intensity at 340 nm was calculated using a fitting curve based on triplicate experiments. The KD or the T113C mutant ecDHFR–NADPH complex *was difficult to estimate*.

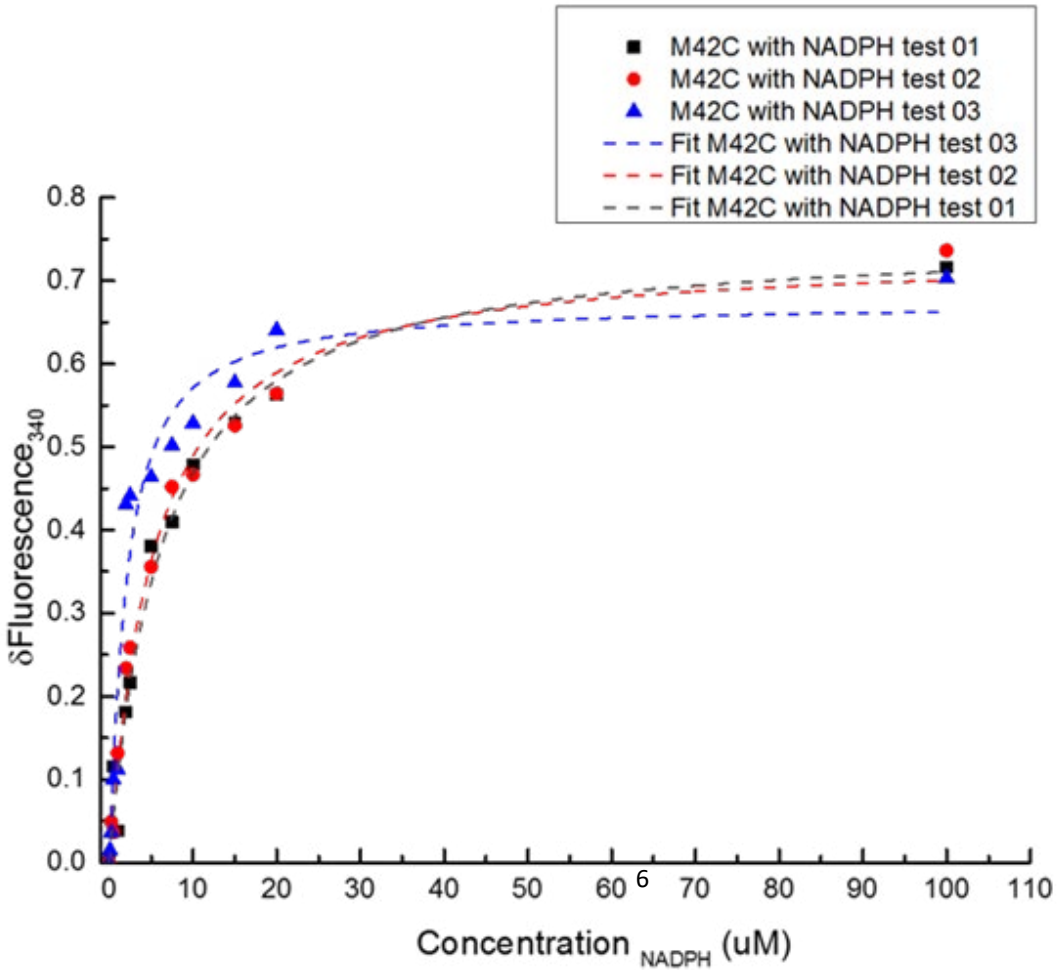


**Figure 1F (3):** The fluorescence emissions for the formation complex of M42C ecDHFR with different NADPH concentrations (0, 0.1, 0.25, 0.5, 1, 2, 2.5, 5.0, 7.5, 10, 15, 20, and 100 μM) under emission 290 nm for triplicate experiments at different times. Fluorescence intensity at 340 nm was calculated using a fitting curve based on triplicate experiments. The KD for the M42C mutant ecDHFR–NADPH complex formation was approximately 4.07 ± 0.58 μM.

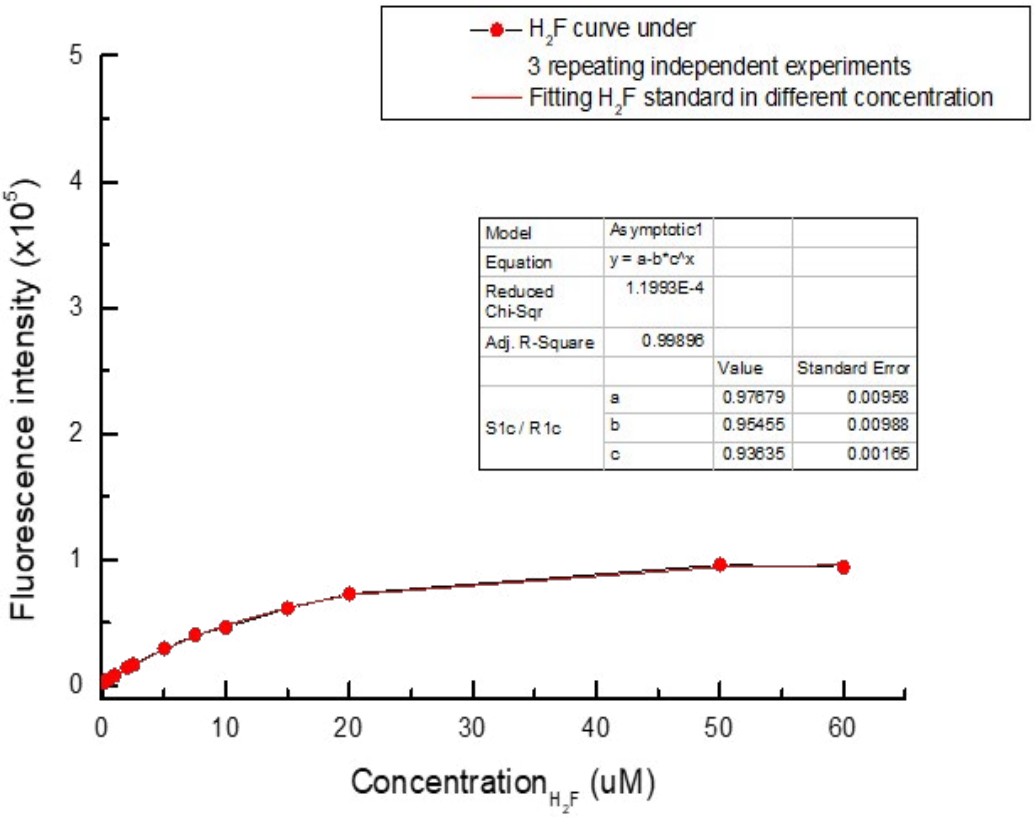


**Figure 1G (4):** Fluorescence counts for different concentrations of H2F (DHF) under MTEN solution. The experimental average fluorescence ratio was fitted with the simulation curve. Each measurement was performed in triplicate, and the results were based on three independent

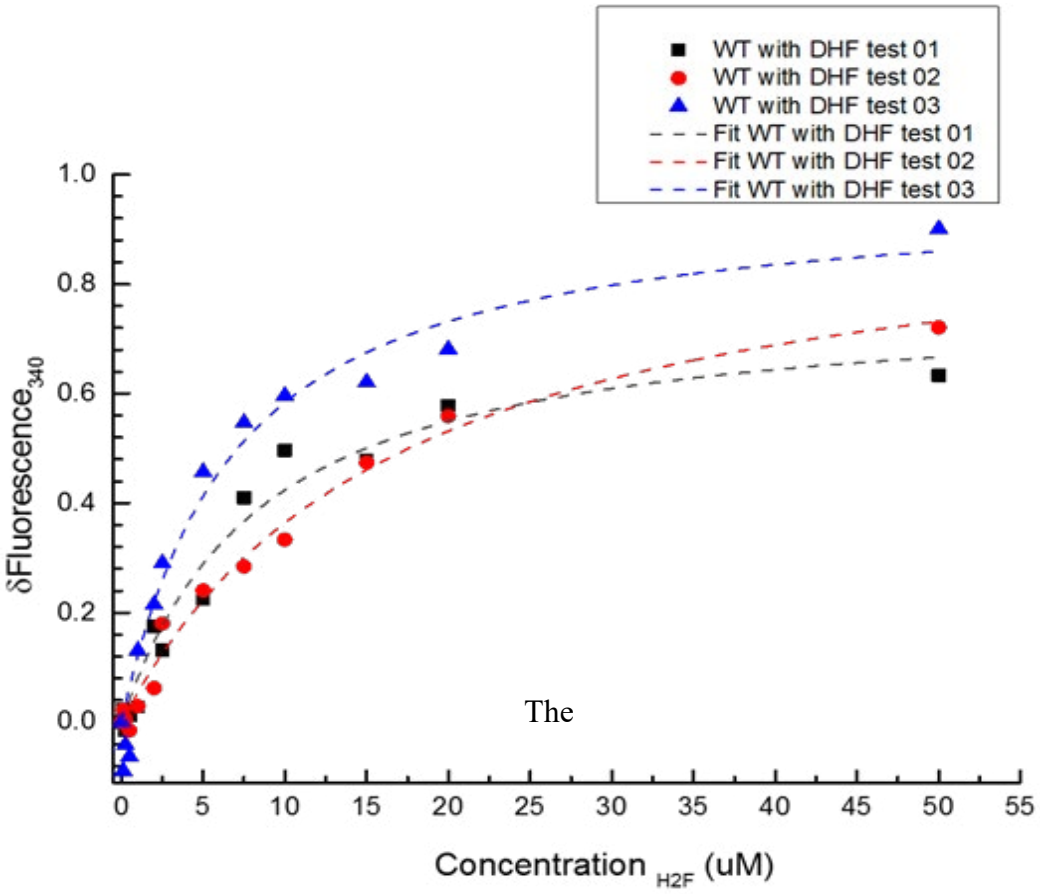


The

**Figure 1G (5):** fluorescence emissions for the formation complex of WT ecDHFR with different DHF concentrations (0, 0.1, 0.25, 0.5, 1, 2, 2.5, 5.0, 7.5, 10, 15, 20, and 50 μM) under emission 290 nm for triplicate experiments at different times. Fluorescence intensity at 340 nm was calculated using a fitting curve based on triplicate experiments. The KD for the wild-type mutant ecDHFR–DHF complex formation was approximately 10.18 ± 1.89 μM

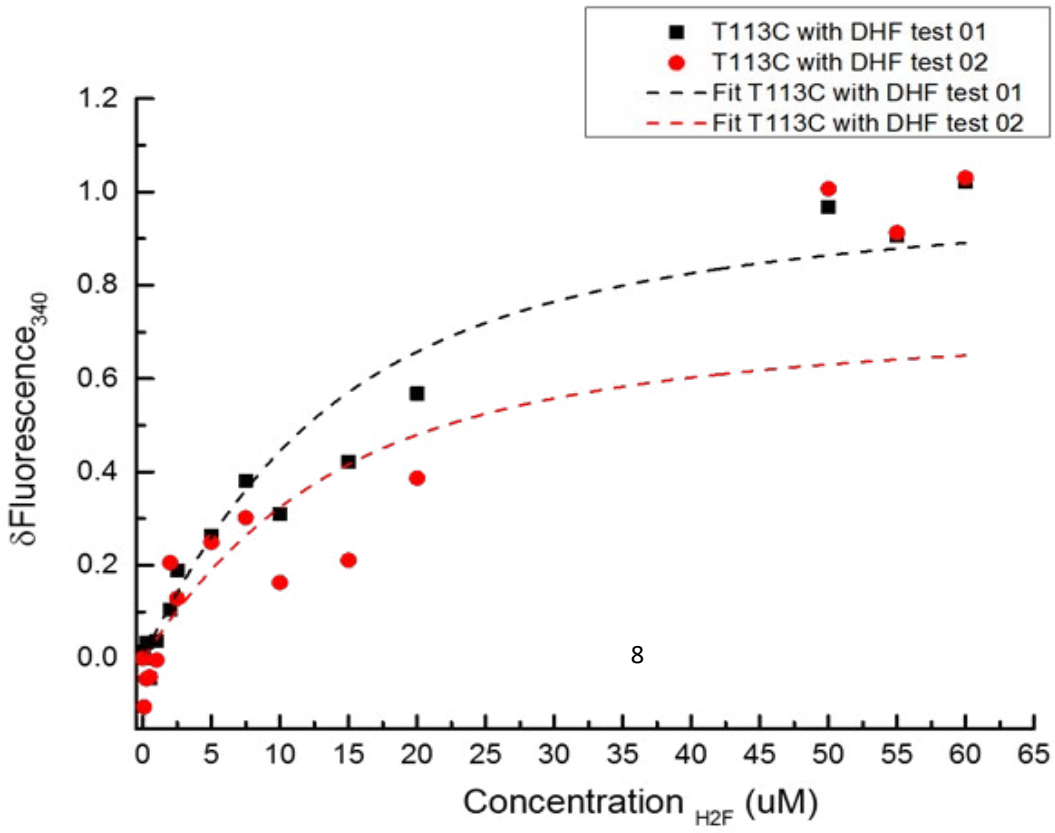


**Figure 1G (7)**

**Figure 1G (7):** The fluorescence emissions for the formation complex of T113C ecDHFR with different DHF concentrations (0, 0.1, 0.25, 0.5, 1, 2, 2.5, 5.0, 7.5, 10, 15, 20, 50, 55, and 60 μM) under emission 290 nm for triplicate experiments at different times. Fluorescence intensity at 340 nm was calculated using a fitting curve based on triplicate experiments. The KD for the wild-type mutant ecDHFR–DHF complex formation was approximately 8.0 ± 0.0 μM.

All data were calibrated with the enzyme at 5 μM ± standard error, resulting in an intensity of 4.5*105 compared to 5.6*105 reported in a previous study [7]. For DHF (H2F), the KD ratio was three times higher compared to the reported value [7]. According to relative amino acid location, three mutants were derived: M42C, W47C, and T113C (Supplementary e.3 (3)).

**Supplementary (e.3) Schematic diagram of X-ray crystallography ecDHFR and interior contents**

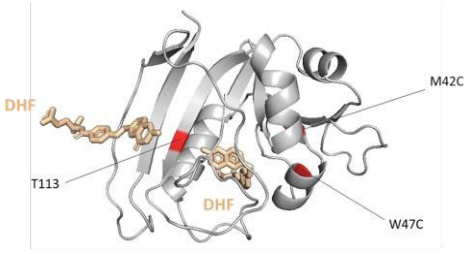


**(1) WT DHFR (PDB: 1rf7) binding with DHF structure**

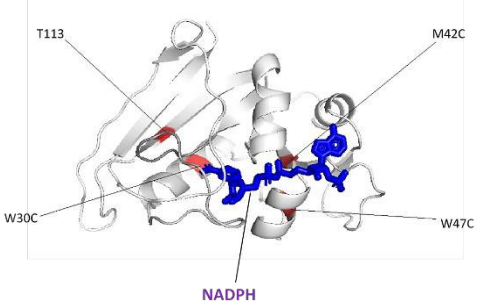


**(2) WT DHFR (PDB: 1rx1) binding with NADPH structure.**

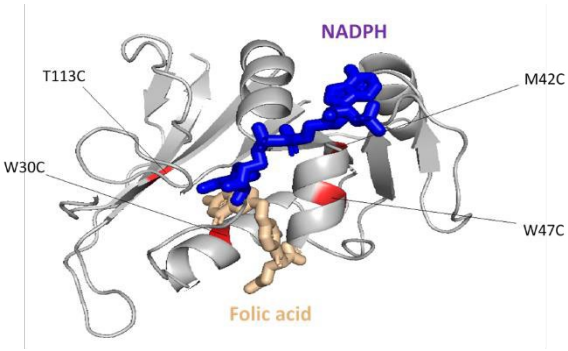


**(3) WT DHFR (PDB: 1RX2) binding with NADPH and DHF structure.**

UV detection at 282 nm was used to analyze the pure compound and the formation complex, but fluorescence spectral data were also required. Clone experiments were conducted using three mutants, namely M42C, W47C and T113C. There was a dramatically increase in the $K_D$ ratio of mutants comparing to wild-type. Therefore, mutations that enhance NADPH-DHFR complex formation were rare in M42C and W47C locations. Apart from the solution effect, conquering the activation energy was a related challenge. However, the findings highlighted the appearance of disulfide bonding in the nearby mutants M42C and W47C. In contrast, the $K_D$ ratio of the enzyme-NADPH complex $K_D$ ratio increase only for M42C, where the KD ratio was approximately $4.07 \pm 0.58$ μM. This structure resembled a "knot" that locked both sides together, resulting in tighter NADPH channels compared with the mutants M42F and W47C. The experiment then focused on detecting DHF-DHFR complex formation detection.

As DHF was not directly linear in its optical properties, recording DHF alone DHF alone a high concentration was necessary to obtain a good linear standard curve. As a result, detecting the $K_D$ ratio for W47C and M42 proved difficult because the two amino acids were far from DHF, leading to no noticeable impact on the tightness or the looseness of the substrate channel. In the case of the farthest mutant is T113C, the $K_D$ ratio of the DHF-DHFR complex was $13.73 \pm 1.82$. The T113C mutant did not yield a idealize $K_D$ ratio when DHFR bound with NADPH or DHF. This discrepancy was suspected to be caused by the farest cysteine residue, which seemingly did not affect complex formation torsion strength.

### 3.2 Changes in Fluorescence Spectrum

After continually adding NADPH and increasing its concentration, the fluorescence of NADPH-DHF was saturated, appearing like a plateau. The fluorescence ratio decreased gradually owing to the formation of hydrogen bonding and ionic bonding from the diluted NADPH in the MTEN buffer and high concentration cofactor, resulting in a quenching effect. Additionally, in the spectral regions of 330-360 nm and 420-460 nm, distinct blue and red-shift, respective become evident with the change in concentration. These shifts explain the weakening of the fluorescence resonance effect. In the DHF-DHFR binding complex formation experiment, DHF is a highly emissive substance that cannot be directly observed at 340 nm excitation. Therefore, 290 nm was used for data collection. DHF exhibits a unique pattern in the spectrum because it is not a linear spectrum when determined concentrations were ranging from 20 to 60 μM. Consequently, the fluorescence spectra displayed complex peaks and background calibration was required. Considering the highly emitting nature of DHF. A red-shift effect was observed in the 330-360nm region.

### 3.3 Electrostatic Attraction of ecDHFR and Mutants: Analysis of an Instant Steady States and Wave Signal Pattern

The steady-state x-crystal data (1rx2) and (1rf7) were calculated for ecDHFR and the mutants; the results are shown in Figs. 1H and 1J (and Supplementary e.8).

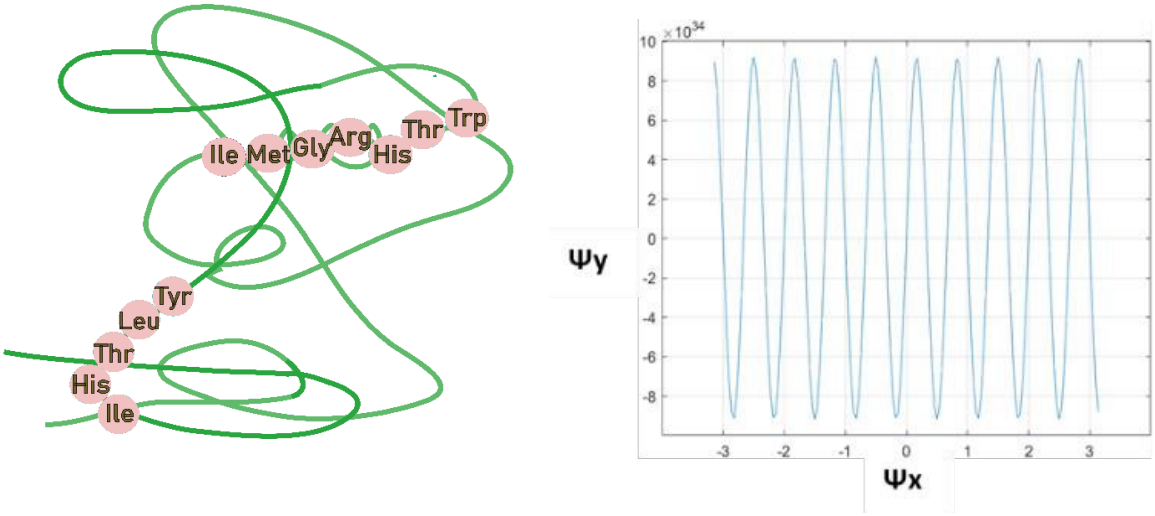


**Figure 1H (1):** The schematic representation of ecDHFR without any substrates and under anhydrous condition. The experiment considers only with ecDHFR and the interior multiple bond forces without any hydrogen interference. The results confirm that both particles, Seg01-1 +Seg02-1 and Seg01-2 + Seg02-1, exhibit the same relative spatial loci and wave function within the system.

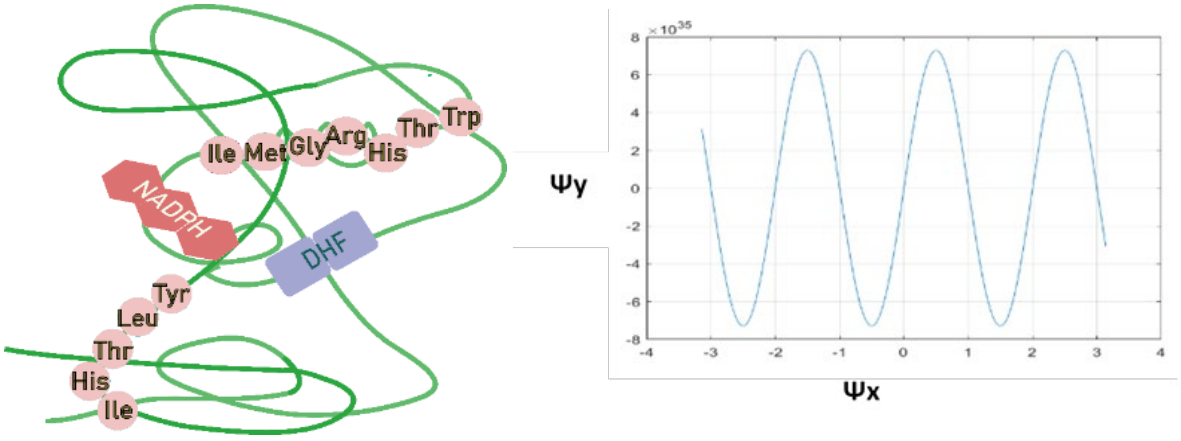


**Figure 1H (2):** The schematic representation of ecDHFR with substrates and under anhydrous condition. The experiment explores ecDHFR with two substrates, considering the interior multiple bonds without any hydrogen interference. The results confirm that both particles, Seg01-1 + Seg02-1 and Seg01-2 + Seg02-1, exhibit the same relative spatial loci and wave function within the system.

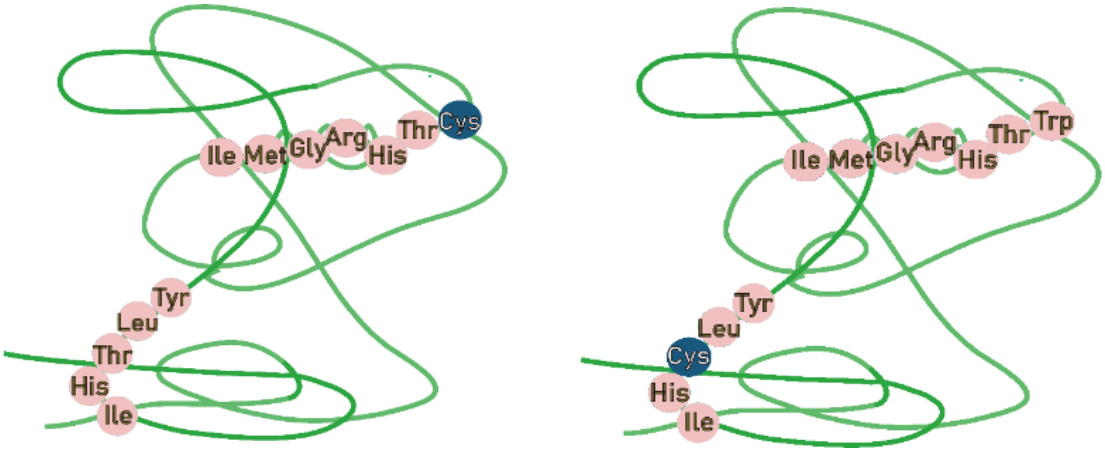


**Figure 1H (3):** The Schematic representation of Seg01-3 + Seg02-1 and Seg01-1 + Seg02-2. Upon analysis, the wave signal intensity and the periodic amplitude are the same as those of Seg01-1 + Seg02-1 and Seg01-2 + Seg02-1.

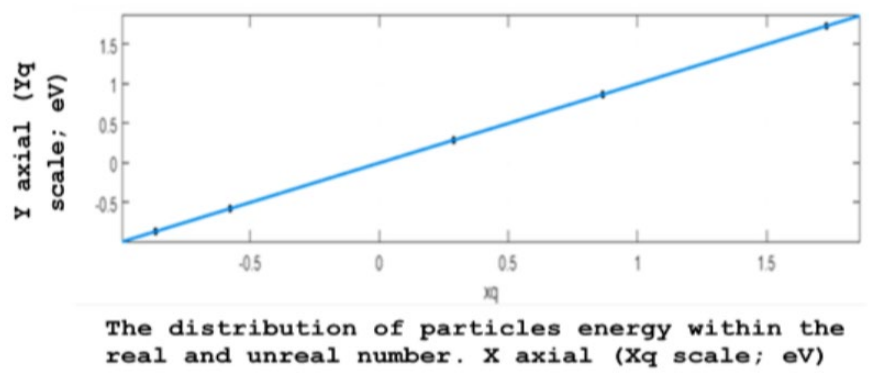


Linear Model Polynominal
f(x) = p1*x3 + p2*x2 + p3*x + p4
where x is normalized by mean -3.172e-17 and
std 1 Coefficients (with 95% confidence bounds):
p1 = 1.812e-16 (-2.287e-16, 5.911e-16)
p2 = -1.81e-16 (-7.741e-16, 4.12e-16)
p3 = 1 (1, 1)
p4 = -0 (-3.387e-16, 3.387e-16)
Goodness of fit:
R-square: 0.99
RMSE: 1.282e-16
SSE: 4.93e-32

It was assumed that mimicry-system-size particles were created from distinct parts of the DHFR fragments after processing the DHFR leading to the following abbreviations. Sequence of wild-type DHFR (Seg WT) = Seg01-1 + mid sequence+ Seg02-1 =Seg01-1 + Seg02-1, (Seg W30C) =Seg01-2 + Seg02-1, (Seg W47C) =Seg01-3 + Seg02-1, (Seg T113C) =Seg01-1 + Seg___. The system size before adding substrates was a = 12.11 Å, b = 40.98 Å, and c = 13.25 Å. After including all the elements, the system size was a = 11.31 Å, b = 38.41 Å, c = 15.89 Å. Using the *Schrödinger equation* and *theory* (Supplementary e.5), after the data were transformed into MATLAB code to analyze a series of instant status loci on different mutant of wave signal. Figure.1H (1)

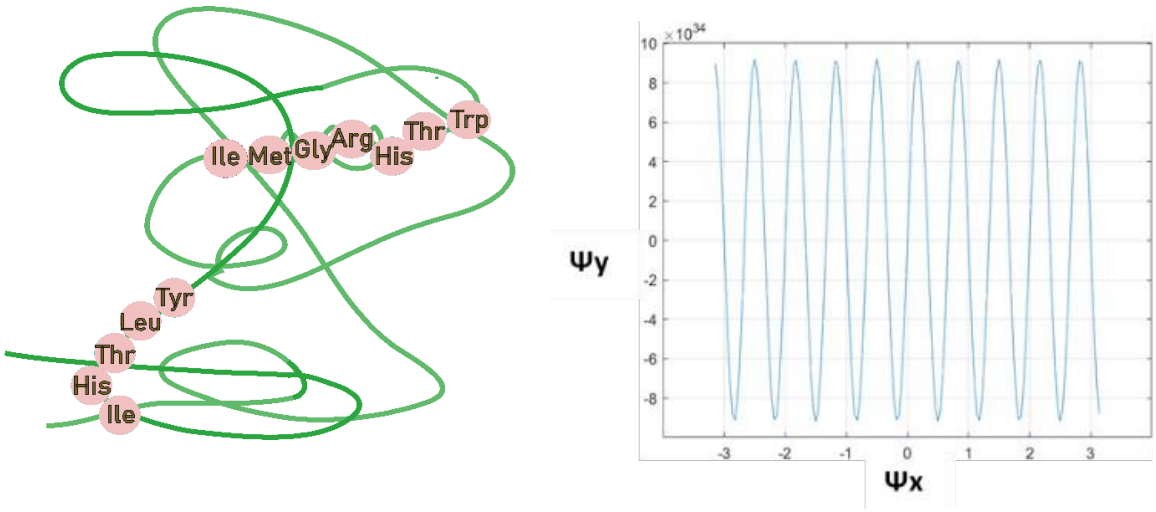


**Figure 1H (1):** The schematic representation of ecDHFR without any substrates and under anhydrous condition. The experiment considers only with ecDHFR and the interior multiple bond forces without any hydrogen interference. The results confirm that both particles, Seg01-1 + Seg02-1 and Seg01-2 + Seg02-1, exhibit the same relative spatial loci and wave function within the system.

showed a tighter signal on the periodic wave before substrates addiction, possibly owing to automatic conformational changes following the response. When the substrate was present, the ecDHFR wave become more relaxed but stronger than the empty ecDHFR (before the reaction) shown in Figure.1H (2), with a difference of approximately 62*x$10^{34}$.

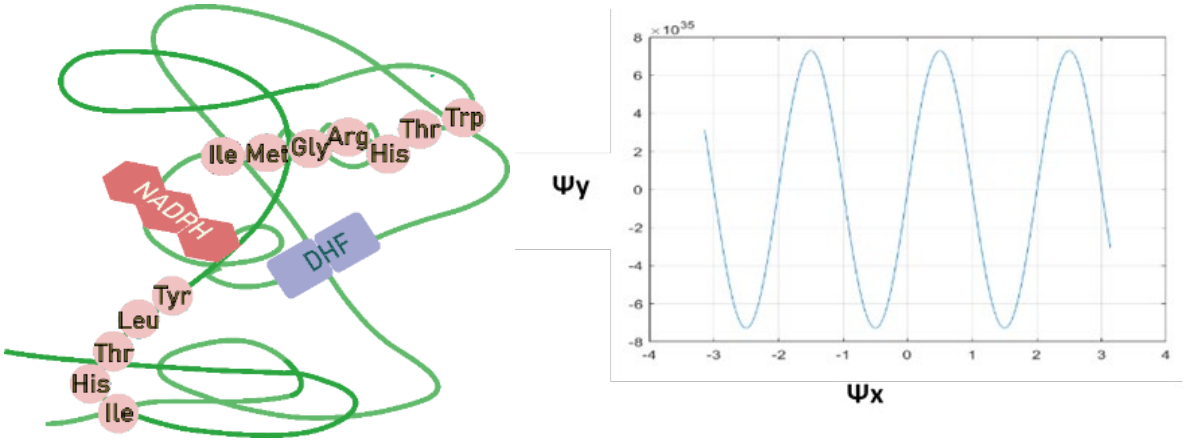


**Figure 1H (2)**: The schematic representation of ecDHFR with substrates and under anhydrous condition. The experiment explores ecDHFR with two substrates, considering the interior multiple bonds without any hydrogen interference. The results confirm that both particles, Seg01-1 + Seg02-1 and Seg01-2 + Seg02-1, exhibit the same relative spatial loci and wave function within the system.

This indicates that a relaxed ecDHFR is easier to read under the conformation change comparing to the steady state without substrates entry. Interestingly, the wave patterns of, Seg01-1 + Seg02-1 and Seg01-2 + Seg02-1 were the same as those of Seg01-3 + Seg02-1 and Seg01-1 + Seg02-2, respectively. This implies that differences were noted only in reactions between different instant statuses from wave signals, whereas the electrostatic effects owing to different mutants were not noticeable.

### 3.4 Electrostatic Attraction of ecDHFR and Mutant in Different Instant Steady States and the Impact on Required Potential Energy

This assumption is also based on the previous discussion, which stated that near- system-size particles were created from different parts of the DHFR mutants' fragment. The Schrödinger equation (Supplementary e.5) was further applied to assess the potential energy in different instant states. Using X-ray crystallography data (1rx2) and (1rf7), two particles were categorized from mutants (Seg01-3 + Seg02-1 and Seg01-1 + Seg02-2) and original particle Seg01-1 + Seg02-1. The ratios were separated into two parts: before the reaction (empty ecDHFR) and after the reaction (saturated ecDHFR). This allowed us to estimate theoretical and realistic ratios to establish a reference. Using all the ratios, a matrix with six columns and 25 rows of data was constructed (Supplementary e.6).

## (e.6) Construction from (e.5) Data Potential and Loci into a Matrix

```
% Files:     CODEReal2C1VXFNHO2
%      Created by:
תבו אי רוני ,אנג'צ יוניס
Acknolwledge to: תבו אי רוני (Massacusetts Institute of Technology)

%
% Entries indicate an interaction between a group of unit and the value
% Represents the interaction cost.
% EOM 3-dim Plates
% ************************************************************************
EOMt1_size = 25; EOMr1_size = 25; EOMt2_size = 25; EOMr2_size = 25; EOMt3_size = 25; EOMr3_size
= 25;
% number of elements in the EOM
system.name = 'state=stn(x,y,z)';n=1;2;3;
system.xvar = 'x_stn';
system.yvar = 'y_stn';
system.yvar = 'z_stn';
eomtn = unique(x,y,z);
eomrn = unique(x,y,z);
% ***** EOM ENTRIES *****
EOMt1(1,1,1)      = -1.4285E-117;
EOMr1(1,1,1)      =    8.8364E-104;
EOMt2(1,1,1)      = -8.8604E-104;
EOMr2(1,1,1)      = -8.8604E-104;
EOMt3(1,1,1)      =    0.0000E+00;
EOMr3(1,1,1)      = -2.7895E-115;
EOMt1(1,1,2)      = -5.7139E-117;
EOMr1(1,1,2)      =    0.0000E+00;
EOMt2(1,1,2)      = -1.0170E-115;
EOMr2(1,1,2)      =    0.0000E+00;
EOMt3(1,1,2)      =    0.0000E+00;
EOMr3(1,1,2)      = -1.1158E-114;
EOMt1(1,2,1)      = -5.7139E-117;
EOMr1(1,2,1)      =    0.0000E+00;
EOMt2(1,2,1)      = -1.0170E-115;
EOMr2(1,2,1)      =    0.0000E+00;
EOMt3(1,2,1)      =    0.0000E+00;
EOMr3(1,2,1)      = -1.1158E-114;
EOMt1(2,1,1)      = -5.7139E-117;
EOMr1(2,1,1)      =    0.0000E+00;
EOMt2(2,1,1)      = -1.0170E-115;
EOMr2(2,1,1)      =    0.0000E+00;
EOMt3(2,1,1)      =    0.0000E+00;
EOMr3(2,1,1)      = -1.1158E-114;
EOMt1(1,2,2)      = -7.1424E-117;
EOMr1(1,2,2)      =    6.7858E-116;
```

EOMt2(1,2,2) = -1.2712E-115;
EOMr2(1,2,2) = 0.0000E+00;
EOMt3(1,2,2) = 0.0000E+00;
EOMr3(1,2,2) = -1.3948E-114;
EOMt1(2,2,1) = -7.1424E-117;
EOMr1(2,2,1) = 6.7858E-116;
EOMt2(2,2,1) = -1.2712E-115;
EOMr2(2,2,1) = 0.0000E+00;
EOMt3(2,2,1) = 0.0000E+00;
EOMr3(2,2,1) = -1.3948E-114;
EOMt1(2,1,2) = -7.1424E-117;
EOMr1(2,1,2) = 6.7858E-116;
EOMt2(2,1,2) = -1.2712E-115;
EOMr2(2,1,2) = 0.0000E+00;
EOMt3(2,1,2) = 0.0000E+00;
EOMr3(2,1,2) = -1.3948E-114;
EOMt1(1,1,3) = 5.7589E-119;
EOMr1(1,1,3) = 6.7858E-116;
EOMt2(1,1,3) = -1.1992E-115;
EOMr2(1,1,3) = 0.0000E+00;
EOMt3(1,1,3) = 0.0000E+00;
EOMr3(1,1,3) = -1.3948E-114;
EOMt1(1,3,1) = 5.7589E-119;
EOMr1(1,3,1) = 6.7858E-116;
EOMt2(1,3,1) = -1.1992E-115;
EOMr2(1,3,1) = 0.0000E+00;
EOMt3(1,3,1) = 0.0000E+00;
EOMr3(1,3,1) = -1.3948E-114;
EOMt1(3,1,1) = 5.7589E-119;
EOMr1(3,1,1) = 6.7858E-116;
EOMt2(3,1,1) = -1.1992E-115;
EOMr2(3,1,1) = 0.0000E+00;
EOMt3(3,1,1) = 0.0000E+00;
EOMr3(3,1,1) = -1.3948E-114;
EOMt1(2,2,2) = 2.3035E-119;
EOMr1(2,2,2) = 2.7143E-116;
EOMt2(2,2,2) = -4.7968E-116;
EOMr2(2,2,2) = 0.0000E+00;
EOMt3(2,2,2) = 0.0000E+00;
EOMr3(2,2,2) = -5.5790E-115;
EOMt1(3,2,1) = 1.3821E-118;
EOMr1(3,2,1) = 1.6286E-115;
EOMt2(3,2,1) = 0.0000E+00;
EOMr2(3,2,1) = 0.0000E+00;
EOMt3(3,2,1) = 0.0000E+00;
EOMr3(3,2,1) = -5.6510E-113;
EOMt1(3,1,2) = 1.3821E-118;
EOMr1(3,1,2) = 1.6286E-115;
EOMt2(3,1,2) = 0.0000E+00;
EOMr2(3,1,2) = 0.0000E+00;
EOMt3(3,1,2) = 0.0000E+00;
EOMr3(3,1,2) = -5.6510E-113;
EOMt1(2,3,1) = 1.3821E-118;
EOMr1(2,3,1) = 1.6286E-115;
EOMt2(2,3,1) = 0.0000E+00;
EOMr2(2,3,1) = 0.0000E+00;
EOMt3(2,3,1) = 0.0000E+00;
EOMr3(2,3,1) = -5.6510E-113;
EOMt1(1,3,2) = 1.3821E-118;

EOMr1(1,3,2) = 1.6286E-115;
EOMt2(1,3,2) = 0.0000E+00;
EOMr2(1,3,2) = 0.0000E+00;
EOMt3(1,3,2) = 0.0000E+00;
EOMr3(1,3,2) = -5.6510E-113;
EOMt1(1,2,3) = 1.3821E-118;
EOMr1(1,2,3) = 1.6286E-115;
EOMt2(1,2,3) = 0.0000E+00;
EOMr2(1,2,3) = 0.0000E+00;
EOMt3(1,2,3) = 0.0000E+00;
EOMr3(1,2,3) = -5.6510E-113;
EOMt1(2,1,3) = 1.3821E-118;
EOMr1(2,1,3) = 1.6286E-115;
EOMt2(2,1,3) = 0.0000E+00;
EOMr2(2,1,3) = 0.0000E+00;
EOMt3(2,1,3) = 0.0000E+00;
EOMr3(2,1,3) = -5.6510E-113;
EOMt1(3,2,2) = 0.0000E+00;
EOMr1(3,2,2) = 9.5001E-116;
EOMt2(3,2,2) = 0.0000E+00;
EOMr2(3,2,2) = 0.0000E+00;
EOMt3(3,2,2) = 0.00000E+00;
EOMr3(3,2,2) = -1.9527E-114;
EOMt1(2,3,2) = 0.0000E+00;
EOMr1(2,3,2) = 9.5001E-116;
EOMt2(2,3,2) = 0.0000E+00;
EOMr2(2,3,2) = 0.0000E+00;
EOMt3(2,3,2) = 0.0000E+00;
EOMr3(2,3,2) = -1.9527E-114;
EOMt1(2,2,3) = 0.0000E+00;
EOMr1(2,2,3) = 9.5001E-116;
EOMt2(2,2,3) = 0.0000E+00;
EOMr2(2,2,3) = 0.00000E+00;
EOMt3(2,2,3) = 0.0000E+00;
EOMr3(2,2,3) = -1.9527E-114;
EOMt1(4,1,1) = 0.0000E+00;
EOMr1(4,1,1) = 8.1429E-116;
EOMt2(4,1,1) = 0.0000E+00;
EOMr2(4,1,1) = 0.00000E+00;
EOMt3(4,1,1) = 0.0000E+00;
EOMr3(4,1,1) = -1.6737E-114;
EOMt1(1,4,1) = 0.0000E+00;
EOMr1(1,4,1) = 8.1429E-116;
EOMt2(1,4,1) = 0.0000E+00;
EOMr2(1,4,1) = 0.00000E+00;
EOMt3(1,4,1) = 0.0000E+00;
EOMr3(1,4,1) = -1.6737E-114;
EOMt1(1,1,4) = 0.0000E+00;
EOMr1(1,1,4) = 8.1429E-116;
EOMt2(1,1,4) = 0.0000E+00;
EOMr2(1,1,4) = 0.00000E+00;
EOMt3(1,1,4) = 0.0000E+00;
EOMr3(1,1,4) = -1.6737E-114;
EOMt1(3,3,1) = 0.0000E+00;
EOMr1(3,3,1) = 9.5001E-116;
EOMt2(3,3,1) = 0.0000E+00;
EOMr2(3,3,1) = 0.00000E+00;
EOMt3(3,3,1) = 0.0000E+00;
EOMr3(3,3,1) = -1.9527E-114;

```
EOMt1(3,1,3)      =    0.0000E+00;
EOMr1(3,1,3)      =    9.5001E-116;
EOMt2(3,1,3)      =    0.00000E+00;
EOMr2(3,1,3)      =    0.00000E+00;
EOMt3(3,1,3)      =    0.0000E+00;
EOMr3(3,1,3)      = -1.9527E-114;
EOMt1(1,3,3)      =    0.0000E+00;
EOMr1(1,3,3)      =    9.5001E-116;
EOMt2(1,3,3)      =    0.0000E+00;
EOMr2(1,3,3)      =    0.00000E+00;
EOMt3(1,3,3)      =    0.0000E+00;
EOMr3(1,3,3)      = -1.9527E-114;

function
[]=eom_matrix;[x_t1,x_r1,x_t2,x_r2,x_t3,x_r3,y_t1,y_r1,y_t2,y_r2,y_t3,y_r3,z_t1,z_r1,z_t2,z_r2,z_t3,z_r3];
            []==eom_matrix;[x_ graph_theoryt1,x_ graph_Realr1,x_ graph_theoryt2,x_ graph_Realr2,x_
graph_theoryt3,x_ graph_Realr3, x_s^-1; y_ graph_theoryt1,y_ graph_Realr1,y_ graph_theoryt2,y_
graph_Realr2,y_ graph_theoryt3,y_ graph_Realr3, y_s^-1;z_ graph_theoryt1,z_ graph_Realr1, z_s^-1;z_
graph_theoryt2,z_ graph_Realr2,z_ graph_theoryt3,z_ graph_Realr3;print_flag,Cluster_matrix];
% [] =graph_matrix[matrix,x_title,y_title,graph_title];
%
%     Function to graph the eom or cluster matrix.
%     The data is plotted as a scatter graph and the size and color
%     Of the marks are conrtrolled according to the value of the input
%
%               Inputs:
%                         matrix          to be plotted on scatter graph
%                         x_theory        string containing label for x-axis
%                         x_ Real
%                         y_theory        string containing label for y-axis
%                         y_ Real
%                         z_theory        string containing label for y-axis
%                         z_ Real
%                         Distribution        title for the graph
%                         x_s^-1              labels to be placed along the x-axis
%                         y_s^-1              labels to be placed along the y-axis
%                         print_flag          flag to toggle printing 1=print, else no print
%                         Cluster_matrix  Optional Cluster_matrix of plotting the clusterd EOM
%
%               Outputs:
% File:       CODEReal2C1VXFNHO2.m
% Created by: אנג'צ יוניס, תבו אי רוני
Acknolwledge to: תבו אי רוני (Massacusetts Institute of Technology)
%     Date: May 20th, 2023
%
%     Function to graph the EOM matrix or cluster matrix.    If the EOM matrix
%     is to plotted in clustered form, the cluster matrix must also be provided.
% Do we hit plotting cluster boxes?
system.name = 'state=stn(x,y,z)';n=1;2;3;
system.xvar = 'x_stn';
system.yvar = 'y_stn';
system.yvar = 'z_stn';
% function fout= eom_tn = unique(x,y,z) = a;
% function fout= eom_rn = unique(x,y,z) = b;
% function fout= eom_tn' = unique(x,y,z) = c;
% function fout= eom_rn' = unique(x,y,z) = d;
% function fout= eom_tn'' = unique(x,y,z) = e;
% function fout= eom_rn'' = unique(x,y,z) = f;
if nargin>3
```

```
    fout= a+c+e; %#ok<NASGU>
    Cluster_plot = -5.00E-116< a+c+e< 0.00E+00; %#ok<NASGU>
else if nargin>3 %#ok<ALIGN>
    fout= b+d+f; %#ok<NASGU>
    Cluster_plot = -6.00E-115< b+d+f< -2.00E-106;
end
[row_input, column_out, m_value] = find(matrix);        % find non_zero entries
max_row = max(row_input);
max_col = max(column_out);
ax = [0 max_col+1 0 max_row+1];
max_value = max(m_value);
data_scale = cell(50/max_value)/20;
x_tcklabel_g{1,1} = '0';
y_tcklabel_g{1,1} = '0';
z_tcklabel_g{1,1} = '0';
for i = 1:size(x_tcklabel,1) %#ok<USENS>
    x_tcklabel_g{i+1,1} = x_tcklabel{i,1};
end
for i = 1:size(y_tcklabel,1) %#ok<USENS>
    y_tcklabel_g{i+1,1} = y_tcklabel{i,1};
end
for i = 1:size(z_tcklabel,1) %#ok<USENS>
%     Function to graph the eom or cluster matrix.
%     The data is plotted as a scatter graph and the size and color
%     Of the marks are conrtrolled according to the value of the input
%
%                 Inputs:
%                             matrix              to be plotted on scatter graph
%                             x_theory            string containing label for x-axis
%                             x_ Real
%                             y_theory            string containing label for y-axis
%                             y_ Real
%                             z_theory            string containing label for y-axis
%                             z_ Real
%                             Distribution            title for the graph
%                             x_s^-1                  labels to be placed along the x-axis
%                             y_s^-1                  labels to be placed along the y-axis
%                             print_flag              flag to toggle printing 1=print, else no print
%                             Cluster_matrix    Optional Cluster_matrix of plotting the clusterd EOM
%
%                 Outputs:
% File:       CODEReal2C1VXFNHO2.m
% Created by: אנג'צ יוניס, תבו אי רוני
Acknolwledge to: תבו אי רוני (Massacusetts Institute of Technology)
%     Date: May 20th, 2023
%
%     Function to graph the EOM matrix or cluster matrix.    If the EOM matrix
%     is to plotted in clustered form, the cluster matrix must also be provided.
% Do we hit plotting cluster boxes?
system.name = 'state=stn(x,y,z)';n=1;2;3;
system.xvar = 'x_stn';
system.yvar = 'y_stn';
system.yvar = 'z_stn';
% function fout= eom_tn = unique(x,y,z) = a;
% function fout= eom_rn = unique(x,y,z) = b;
% function fout= eom_tn' = unique(x,y,z) = c;
% function fout= eom_rn' = unique(x,y,z) = d;
% function fout= eom_tn'' = unique(x,y,z) = e;
% function fout= eom_rn'' = unique(x,y,z) = f;
```

```
if nargin>3
    fout= a+c+e; %#ok<NASGU>
    Cluster_plot = -5.00E-116< a+c+e< 0.00E+00; %#ok<NASGU>
else if nargin>3 %#ok<ALIGN>
    fout= b+d+f; %#ok<NASGU>
    Cluster_plot = -6.00E-115< b+d+f< -2.00E-106;
end
[row_input, column_out, m_value] = find(matrix);        % find non_zero entries
max_row = max(row_input);
max_col = max(column_out);
ax = [0 max_col+1 0 max_row+1];
max_value = max(m_value);
data_scale = cell(50/max_value)/20;
x_tcklabel_g{1,1} = '0';
y_tcklabel_g{1,1} = '0';
z_tcklabel_g{1,1} = '0';
for i = 1:size(x_tcklabel,1) %#ok<USENS>
    x_tcklabel_g{i+1,1} = x_tcklabel{i,1};
end
for i = 1:size(y_tcklabel,1) %#ok<USENS>
    y_tcklabel_g{i+1,1} = y_tcklabel{i,1};
end
for i = 1:size(z_tcklabel,1) %#ok<USENS>
    z_tcklabel_g{i+1,1} = z_tcklabel{i,1};
end
figure;
clf;
scatter(column_out, row_input, m_value*data_scale, m_value,'filled','d');
axis(ax);
cur_ax = gca;
axes_scale = get(cur_ax,'Position');
set(cur_ax,'Position',[axes_scale(1) axes_scale(2) axes_scale(3) axes_scale(4)*0.9]);
set(cur_ax,'XTick',(0:1:max_col+1));
set(cur_ax,'YTick',(0:1:max_row+1));
set(cur_ax,'XAxisLocation','top','YDir','Reverse');
set(cur_ax,'XTickLabelMode','manual');
set(cur_ax,'YTickLabelMode','manual');
set(cur_ax,'XTickLabel',x_tcklabel_g);
set(cur_ax,'XTickLabel',y_tcklabel_g);
set(cur_ax,'YTickLabel',z_tcklabel_g);
set(cur_ax,'FontSize',4);
set(cur_ax,'Box','On');
xlabel(x_title);
ylabel(y_title);
zlabel(z_title);
title(graph_title);
orient('landscape');
% draw squares around the clustered elements in the DSM
if Cluster_plot ==1
    Number_clusters = size(Cluster_matrix,1);
    sq_s = 0.5;    %Start of the square
    for cluster_indx = 1:Number_clusters
n_el = sum(Cluster_matrix(cluster_indx,:),2);          % number of elements in cluster line([sq_s (sq_s + n_el)
(sq_s + n_el) sq_s sq_s], [sq_s (sq_s + n_el) (sq_s + n_el) sq_s]);
        sq_s = sq_s + n_el;
    end
end
if print_flag ==1
    print
end
```

The six columns were labeled T1, R1, T2, R2, T3, and R3 (T = theory, R = real), and the 25 rows represented different excitation states, ranging from the ground state (1,1,1) to a certain level of excitation (3, 3, 1), (3, 1, 3), (1, 3, 3). These data were calculated and categorized. A simple combination was executed by clustering different system parts of wild-type and mutant ecDHFR particles with potential input at different loci. A deferential partition function ensured that the theoretical and realistic potential energy under the same system size (reaction and empty) exhibited a linearly relationship with the particle conformation in wild-type and mutant ecDHFR (figure. 1J).

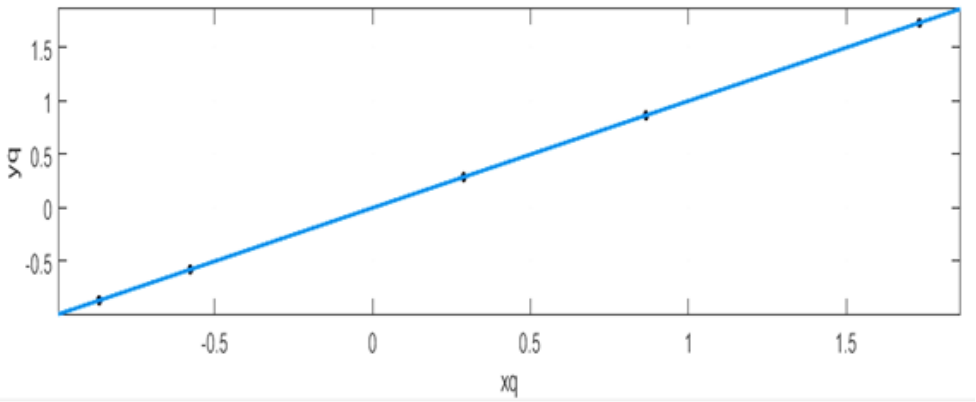


Linear Model Polynominal
f(x) = p1*x3 + p2*x2 + p3*x + p4
where x is normalized by mean -3.172e-17 and
std 1 Coefficients (with 95% confidence bounds):
p1 = 1.812e-16 (-2.287e-16, 5.911e-16)
p2 = -1.81e-16 (-7.741e-16, 4.12e-16)
p3 = 1 (1, 1)
p4 = -0 (-3.387e-16, 3.387e-16)
Goodness of fit:
R-square: 0.99
RMSE: 1.282e-16
SSE: 4.93e-32

**Figure 1J:** The steady-state x-crystal (1rx2) and (1rf7) are calculated for ecDHFR and ecDHFR complex predicted potential energy. Linear polynomials curve only applied *qX* and *qY* data.

After analyzing *q*X and *q*Y space distribution data and observing linearity between potential energy before the reaction (theory) and after the reaction (realistic) in two ratios, it became evident that ecDHFR ratios theoretically exhibited a rapid increase in electrostatic attraction from the ground state to the excitation state. However, the real group experienced a gradual descent to a lower equilibrium level, and attraction force became negligible. These findings indicate that the wild-type ecDHFR before reaction (theory group) exhibited a higher adopted energy level when excited compared with mutant ecDHFR, but the reaction in the two types of mutants (real group) was more slowly reflected in the excitation of the potential energy. This behavior change was also reflected in the wave signal alterations, as shown in Fig.1H. However, detecting a higher wave signal in the mutants from to the theory base was still possible compared with the wild type.

## 4. Conclusions

Herein, we explored various parameters influencing the reaction pathways, formation mechanisms, and reaction ratios during an instant reaction between ecDHFR from wild-type and mutant strains of E. coli and different substrates. Parameters, such as conformation and steric hindrance, electrostatic or hydrophobic-/hydrophilic forces, activation energy, and potential were considered. For the first time, an affinity test was performed on different strains of ecDHFR, and their binding affinity to substrates, including DHF and cofactor NADPH, was lower compared with the wild-type. Furthermore, we analyzed the theoretical electrostatic and potential energy before and after the reactions in different ecDHFR strains. In the instant steady state, we successfully created the wave signal from the wild type before and after the reaction, demonstrating that the signal was rapidly detected in the reaction group compared with the empty one (not reacted). However, the wave signal level

pattern from of the mutant could not be distinguished from that of the wild-type before and after the reaction. This confirms that the pattern remained consistent in W47C and T113C mutants as well as in the wild type and W30C during the reaction.

Furthermore, the experiment assumption and results significantly indicated the potential energies in the nonreaction(theory) and instant reaction (real) states were higher in the wild-type and compared with the other two strains which cladded the substrate, cofactor in the steady state complexes. The higher electrostatic potential energy in the wild type ($E < 0$) implies a faster conformation change and reflection when exposed to external excitation, which is alternated and distribution with the atomic polarity and electricity. Conversely, the mutant exhibited lower attraction at different states ($E \ll 0$), suggesting a slower saturation compared with the wild-type and a higher energy requirement to complete the reaction, and it can be altered by other factor like temperature, or vibration even the applied force. These findings also agree with Schrödinger's theory and support the previous affinity experiment conducted on different wild type ecDHFR mutant strains [8-14].

## References


1. Maurer, B. J., Barker, P. E., Masters, J. N., Ruddle, F. H., & Attardi, G. (1984). Human dihydrofolate reductase gene is located in chromosome 5 and is unlinked to the related pseudogenes. *Proceedings of the National Academy of Sciences,* 81(5), 1484-1488.
2. Kaufman, S. (1967). Metabolism of the phenylalanine hydroxylation cofactor. *Journal of Biological Chemistry*, 242(17), 3934-3943.
3. Charlton, P. A., Young, D. W., Birdsall, B., Feeney, J., & Roberts, G. C. (1979). Stereochemistry of reduction of folic acid using dihydrofolate reductase. *Journal of the Chemical Society, Chemical Communications,* (20), 922-924.
4. Krahn, J. M., Jackson, M. R., DeRose, E. F., Howell, E. E., & London, R. E. (2007). Crystal structure of a type II dihydrofolate reductase catalytic ternary complex. *Biochemistry*, 46(51), 14878-14888.
5. Maharaj, G., Selinsky, B. S., Appleman, J. R., Perlman, M., London, R. E., & Blakley, R. L. (1990). Dissociation constants for dihydrofolic acid and dihydrobiopterin and implications for mechanistic models for dihydrofolate reductase. *Biochemistry*, 29(19), 4554-4560.
6. Sawaya, M. R., & Kraut, J. (1997). Loop and subdomain movements in the mechanism of Escherichia coli dihydrofolate reductase: crystallographic evidence. *Biochemistry*, 36(3), 586-603.
7. Huang, C. H., Chen, Y. W., Huang, T. T., & Kao, Y. T. (2021). Effects of distal mutations on ligand-binding affinity in E. coli dihydrofolate reductase. *ACS omega*, 6(40), 26065-26076.
8. Bolin, J. T., Filman, D. J., Matthews, D. A., Hamlin, R. C., & Kraut, J. (1982). Crystal structures of Escherichia coli and Lactobacillus casei dihydrofolate reductase refined at 1.7 A resolution. I. General features and binding of methotrexate. *Journal of Biological Chemistry*, 257(22), 13650-13662.
9. Basset, G. J., Quinlivan, E. P., Ravanel, S., Rébeillé, F., Nichols, B. P., Shinozaki, K., ... & Hanson, A. D. (2004). Folate synthesis in plants: the p-aminobenzoate branch is initiated by a bifunctional PabA-PabB protein that is targeted to plastids. *Proceedings of the National Academy of Sciences*, 101(6), 1496-1501.
10. Lakowicz, J. R. (Ed.). (2006). *Principles of fluorescence spectroscopy*. Boston, MA: springer US.
11. Neuburger, M., Rébeillé, F., Jourdain, A., Nakamura, S., & Douce, R. (1996). Mitochondria Are a Major Site for Folate and Thymidylate Synthesis in Plants, *Journal of Biological Chemistry*, 271(16), 9466-9472.
12. Salcedo, E., Cortese, J. F., Plowe, C. V., Sims, P. F., & Hyde, J. E. (2001). A bifunctional dihydrofolate synthetase–folylpolyglutamate synthetase in Plasmodium falciparum identified by functional complementation in yeast and bacteria. *Molecular and biochemical parasitology*, 112(2), 239-252.
13. B. T. K. Tresvant B. Goodwin, Rita C. Gardine, *the journal of biological chemistry*, 1966, 241, 1319-1328.
14. Williams, J. W., Morrison, J. F., & Duggleby, R. G. (1979). Methotrexate, a high-affinity pseudosubstrate of dihydrofolate reductase. *Biochemistry*, 18(12), 2567-2573.